Theoretical and Experimental Investigations of Rotational CARS as a Technique for Temperature Probing

Diploma Project

by

David Nilsson

Lund Reports on Atomic Physics, LRAP-76,
Lund, May 1987

CONTENTS PAGE

I. Introduction.

This paper is the result of a diploma project for a Master of Science degree in engineering physics at Lund Institute of Technology (LTH). The experiments were carried out at the Department of Atomic Physics at LTH.

This work is part of the effort to make rotational CARS a competitive temperature measurement technique and concentrates on evaluation and noise problems. The main goal has been to adapt and further develop existing computer programs for the generation of theoretical rotational CARS spectra and the prediction of temperature, and then to test these programs. In addition, some properties of several dyes have been examined, e.g. the spectral form, the noise and the effects of dye mixing and how these influence the accuracy when using rotational CARS for thermometry.

Some of the results obtained were presented in one of the posters of our group at the European CARS meeting in Stuttgart, FRG, March 1987. The project will be continued during the late spring of 1987 and hopefully the computer programs will be considerably improved and more thoroughly tested against experimental CARS spectra.

This paper begins with a brief introduction to molecular spectroscopy and CARS theory followed by a survey of the applications of the CARS technique for combustion probing. The following sections focus on different aspects of temperature measurements dealing with the theory involved, the results obtained as well as a discussion of the obstacles encountered.

II. Basic molecular and Raman spectoscopy

As an introduction to the following sections some basic molecular spectroscopy will be presented. (A thorough presentation of molecular spectroscopy is given by, for example, Herzberg in Spectra of Diatomic Molecules [1].) The reason for the complicated nature of molecular spectra is partly the absence of a centre of motion for the electrons and partly the existence of rotational and vibrational motion.

Most of the formulations and notations in the following sections are identical to those of Parameswaran and Snelling [2] in their instructions to the CARS computer code developed by R.J. Hall. As a first approximation the electronic, vibrational and rotational motions are assumed to be independent and the total energy of the molecule can be written as a sum of the three contributions

$$E_{tot} = E_{el} + E_{rot} + E_{vib}$$

Before examining the different degrees of freedom the term is defined as E/hc with dimensions of reciprocal centimetres. (h is Planck's constant and c the velocity of light.) The rotational term is denoted $F_v(J)$ and the vibrational term G(v).

$$F_v(J) = E_{rot} / hc \qquad \text{and} \qquad G(v) = E_{vib} / hc$$

Rotational structure

For a rigid rotating molecule F_v is easily derived from the Schrödinger equation by setting the potential V(r)≡0. This gives

$$F_v(J) = BJ(J+1)$$

where B is the rotational constant and J = 0,1,2,....

For a more realistic nonrigid rotator the expression is

$$F_v(J) = B_v J(J+1) - D_v J^2(J+1)^2$$

, where D_v is the centrifugal distortion constant.

Vibrational structure

When treating vibrational motion the simplest model assumes a harmonic oscillator potential resulting in

$$G(v) = \omega(v+1/2) \quad \text{where } v = 0,1,2,.... \text{ and } \omega \text{ is a constant.}$$

For higher vibrational levels an anharmonic oscillator model is necessary yielding some additional correction terms [2]

$$G(v) = \omega_e (v+1/2) - \omega_e x_e (v+1/2)^2 + \omega_e y_e (v+1/2)^3 + \omega_e z_e (v+1/2)^4$$

where ω_e, $\omega_e x_e$, $\omega_e y_e$ and $\omega_e z_e$ are spectroscopic constants.

The initial assumption of independent degrees of freedom is only approximately valid. A large vibrational motion also effects the rotational motion and a correction of the rotational constants, named the Dunham expansion, is required.

$$B_v = B_e - \alpha_e (v+1/2) + \gamma_e (v+1/2)^2 \quad \text{and}$$

$$D_v = D_e + \beta_e (v+1/2),$$

where, again, α_e, β_e and γ_e are spectroscopic constants.

Selection rules

For an infra-red transition the selecton rules are $\Delta v=+1,-1$ and $\Delta J=+1,-1$. When $\Delta J=-1$ the transitions are called the P branch and for $\Delta J=+1$ the R branch. In this paper, Raman transitions are considered, following $\Delta v=+1,-1$ and $\Delta J=+2$ (S branch),0 (Q branch),-2 (O branch). In a pure rotational Raman transition the selection rule is $\Delta J=+2,-2$.

Hot bands

The anharmonicity of the vibrational potential has the effect that the vibrational transitions $v=0\rightarrow v=1$ and $v=1\rightarrow v=2$ do not coincide in frequency. Due to the small population of higher vibrational states at lower temperatures the effect is only observed at higher temperatures, hence the name hot bands.

A different kind of hot band can occur in a pure rotational spectrum. This is caused by the v dependence of the rotational constant resulting in a deviation in the frequencies of, for example, a $J=1\rightarrow J=3$ transition in the $v=0$ and $v=1$ states.

III. Elements of CARS theory

Coherent Anti-Stokes Raman Scattering (CARS) is a non-linear optical process, first observed by Maker and Terhune [3], where a coherent beam is formed through the interaction of three incident, high-power laser beams with a medium. In the region where light beams with frequencies ω_1, ω_2 and ω_3 overlap (in space and time) radiation is produced with the frequency $\omega_4 = \omega_1+\omega_2-\omega_3$. Because the process is coherent, the emitted beam is highly directional and has a wave vector $k_4 = k_1+k_2-k_3$. In practice, a three-colour experiment is simpler using two lasers as sources so that $\omega_1 \equiv \omega_2$ and $k_4 = 2k_1-k_3$. When one of these lasers is tuned, a strong signal is generated when $\omega_1-\omega_3=\omega_r$, where ω_r is the frequency of a Raman resonance in the medium.

The Raman frequency ω_r may correspond to either a rotational-vibrational or pure rotational transition. The most thorougly investigated case is that of the rotational-vibrational transition and is referred to as vibrational CARS (fig 3.1). In this paper, however, it is the properties of rotational CARS (fig 3.2) spectra that will be treated.

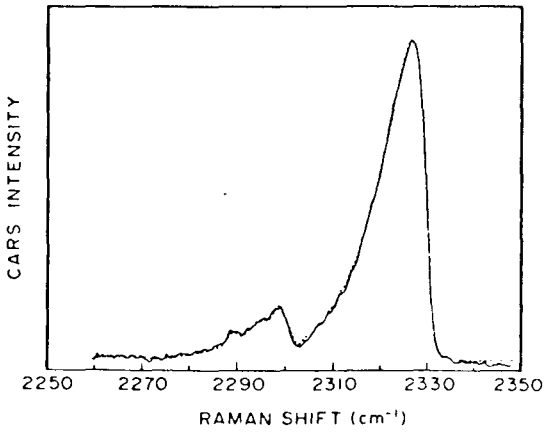

Fig 3.1. Vibrational CARS.

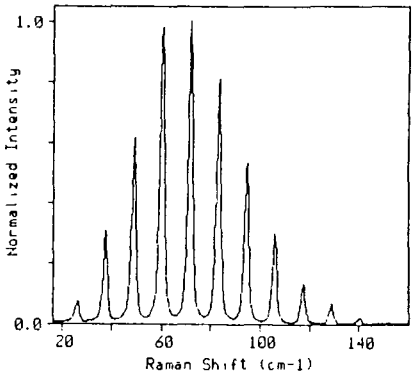

Fig 3.2. Rotational CARS.

It was earlier mentioned how the CARS spectra were obtained by tuning one of the lasers. This is the original method referred to as scanning CARS, and is usually characterized by tuning the Stokes beam frequency. The laser beams are sometimes called the pump and the

Stokes beam. The pump beam in this work was the green Nd:YAG beam used to pump the dye laser, in a scanning CARS set-up it is used twice, $\omega_1=\omega_2$, and the Stokes beam, ω_3, is the dye laser beam.

If a time-resolved measurement is required a single-shot measurement is preferred. This is achieved by using a broad-band Stokes source. (Broad-band CARS, fig. 3.3).

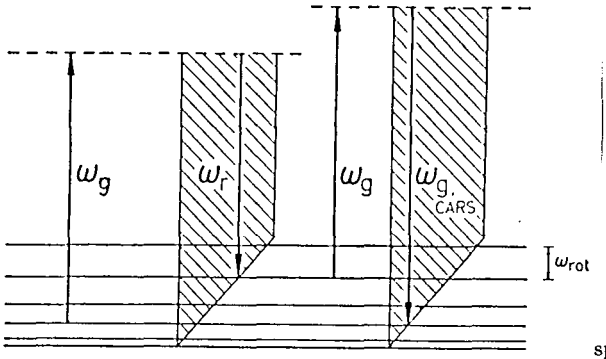

Fig 3.3. Schematic view of the broad-band CARS process.

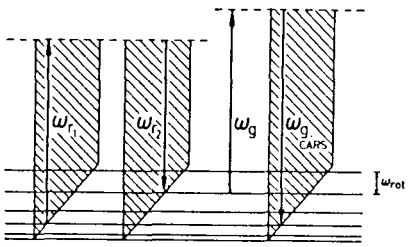

Energy-level diagram for generation of rotational CARS spectra using a multiple four-color interaction process.

Fig 3.4.

If the first pump beam, ω_1, is substituted by another broad-band dye source we get what is called a dual-broad-band configuration [4]. In some recent experiments the two broad-band beams have successfully been taken from the same laser [4,5] (fig 3.4) and this is the method that has been employed when recording the CARS spectra discussed in this paper.

The most obvious experimental CARS set-up utilizes a collinear phase-matching configuration. This leads to difficulties when ω_r is a rotational Raman transition with a small Raman frequency, because of the difficulties in spectrally separating the strong laser beams from the considerably weaker CARS beam. This is the reason why the first reported rotational CARS experiment [6] was performed on H_2 which has a very large rotational constant. (For other important CARS experiments see Refs [7-13].) The remedy is to spatially isolate the CARS signal from the pump and Stokes beams by a three dimensional phase-matching geometry (folded BOXCARS [14,15], fig. 3.5) and/or taking advantage of the fact that differently polarized incident beams result in CARS and pump beams with different polarizations [13].

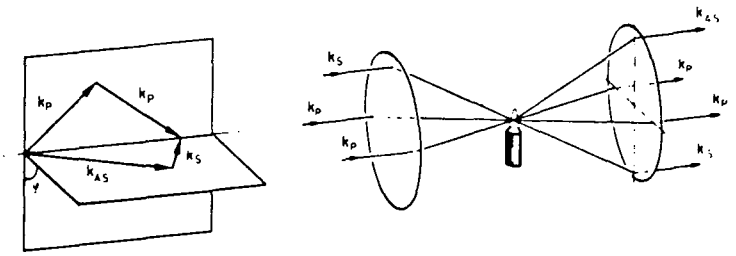

Fig. 3.5. A folded BOXCARS phase-matching geometry.

A distinction is made between the case of a Raman beam shifted towards higher frequency, called CARS (fig. 3.6), and the case of shifts towards lower frequencies, called CSRS (Coherent Stokes Raman Scattering) (fig. 3.7). Most spectra examined here are CSRS spectra.

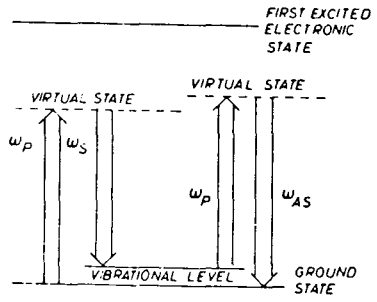

Fig. 3.6. Schematic view of the CARS process.

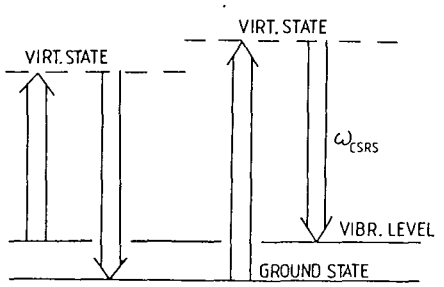

Fig. 3.7. Schematic view of the CSRS process.

CARS generation can be described both classically, using Maxwell's equations, or quantum mechanically, utilizing the density matrix theory [16].

The CARS intensity, I_{aS}, is readily expressed as

$$I_{aS}(\omega_{aS}) = \int f^{slit}(\omega_{aS}-\omega)\, d\omega \iiint |X(\omega'-\omega_p) + X(\omega''-\omega_s)|^2 \times$$

$$\times I_p(\omega')\, I_p(\omega'')\, I_s(\omega_s)\, \delta(\omega_p=\omega'+\omega''-\omega_s)\, d\omega'\, d\omega''\, d\omega_s ,$$

where X is the third-order electrical susceptibility of the medium, f is the slit function of the detection system, I_p is the pump laser intensity, I_s is the Stokes laser intensity and δ is the Dirac-function.

The electrical third-order susceptibility, X, can be divided into a resonant and a non-resonant part,

$$X = X_R + X_{NR} ,$$

where the non-resonant contribution X_{NR} arises mainly from virtual one- and two-photon absorptions in all species present [17]. Theoretical expressions for X are presented in section V iii:1.

IV. Applications of CARS to combustion research

IV i) Introduction

Laser Raman techniques offer a means of performing nonperturbing measurements of medium conditions with high spatial and temporal resolution. For diatomic molecules which are not infra-red active and consequently difficult to detect, Raman scattering and CARS can be particularly important for both concentration and temperature measurements.

In combustion research the CARS diagnostic technique is well suited as a non-intrusive probe, coping with the problems of interference from highly fluorescent compounds. The pioneering CARS experiments on combustion probing were performed by Taran and co-workers in the early 1970's [18,19]. (See also Refs [17,20,21].) The use of physical probes for temperature and species temperature and species concentration measurements can be questionable in many circumstances [17]; they may disturb the medium under investigation, the results may be subject to corrections that are difficult to specify, and they may not even survive especially hostile environments.

IV ii) Methods for temperature probing

In air-fed combustion, N_2 is usually the dominant constituent and will be present nearly everywhere in high concentrations. Consequently, its CARS spectrum will be dominated by the resonant contribution, yielding the temperature of the gas, and the distortions of the spectrum due to the nonresonant background susceptibility will thus normally be small (see Ref. [22], p.226).

At flame temperatures (1000-2000 K) the shape and relative intensities of the rotational-vibrational bands have been shown to be dependable indicators of temperature. At room temperature and below, the CARS Q-branch spectra are less sensitive to small changes in temperature. Instead, pure rotational CARS provides temperature-sensitive spectra. Other advantages with pure rotational CARS are that the rotational lines are well resolved and that almost all rotational spectra of interest can be effectively covered with a single dye.

At higher temperatures the rotational CARS signals are substantionally reduced as the population difference between the initial and final states for the CARS process approaches zero. But the temperature range may possibly be further extended by taking advantage of the increasing presence of rotational hot-band lines above 1300 K. For N_2, the spacing at J=10 is $\approx 0.86 cm^{-1}$ [23] and single-shot temperatures [23,24] could thus be obtained by a much narrower bandwidth dye than that usually required in a Q-branch determination.

In chapter III the dual-broad-band technique was discussed. This is the method used when collecting the CARS (or CSRS) spectra treated in this paper. Unfortunately, the finite dye laser bandwidth introduces a Gaussian envelope into the overall CARS intensity profile with small intensities for large Raman shifts. This limits the method to lower temperatures. Improvements could be made if broader dyes could be developed or if a mixture of two dyes could give a broader profile or even two somewhat separated peaks in the fluorescence curve. This will be further discussed in chapter VI. The method used for temperature evaluation will be discussed in chapter V.

V. Temperature evaluation

V i) Introduction

Due to the non-linear nature of the CARS process and to the asymmetrical lineshape introduced through the interference between the resonant signal and the background ([22], p.226), the temperature evaluation must, in some way, be performed using a computer code. In the following sections various methods will be discussed and one specific method will be discussed in more detail.

V ii) Methods of evaluation

Different methods for temperature evaluation can be found in the literature. The most commonly used procedure for vibrational CARS is to fit complete theoretical spectra, generated in advance, to the experimental spectrum using a library of theoretical spectra for different temperatures.

For rotational CARS, most fitting programs seem to take advantage of the fact that the rotational peaks are well separated and therefore a simpler fitting procedure using only the integrated areas of the Raman lines is possible (fig. 5.1.). However, complications will arise if several species contribute, if the resolution is low or if the background is considerable.

The fitting program developed in this diploma project was developed from an existing program [2] for fitting vibrational CARS spectra, and relatively small modifications have resulted in a functioning program for rotational CARS temperature evaluations.

Another method that has been discussed is to derive the temperature from a study of the Fourier transform of the rotational CARS spectrum [25]. This interesting approach has, however, not been studied in this work.

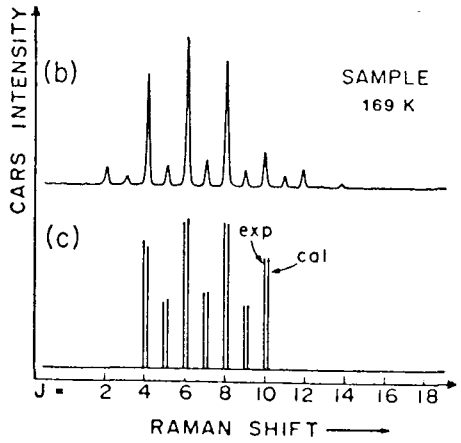

Fig 5.1. Fitting of rotational CARS peak areas [26].

A method for temperature determination from rotational Raman line intensities can be found in [27]. The precision of CARS temperature measurements is treated in [28,29].

V iii) Theory and parameters for the generation of CARS spectra

Some of the expressions and numerical values used in the program package will be explained here. The basic theory of molecular spectra was treated in chapter II and will not be dealt with again. However, it should be mentioned that the values of α_e, β_e, γ_e, ω_e, $\omega_e x_e$, $\omega_e y_e$ and $\omega_e z_e$ employed in the program were found in Ref. [30].

V iii:1) Electrical non-linear susceptibilities

From chapter III, the susceptibility is given by

$$X = X_R + X_{NR}$$

The resonant contribution X_R [22] is given by

$$X_R(\omega) = \frac{N}{\hbar} \sum_j \frac{3}{45} \cdot \frac{b_j^{j'} \gamma_{00}^2 \Delta\rho_{jj'}}{(\omega - \omega_j) - i\Gamma_j/2}$$

where $\hbar$ is Planck's constant/2π, ω is the wave number, ω_j is the Raman resonant wave number and Γ_j is the corresponding Raman linewidth. N is the molecular number density and $\Delta\rho_{jj'}$ is the normalized population difference between the states j and j+2, more explicitly given by

$$\Delta\rho_{JJ'} = (2J+1)\, g_J \exp[-(E(v,J+2)-E(v,J))/kT]/Q$$

for the O-branch (CSRS) and

$$\Delta\rho_{JJ'} = (2J+1)\, g_J \exp[-(E(v,J)-E(v,J-2))/kT]/Q$$

for the S-branch (CARS) , where Q is the partition function and g is a nuclear J dependent spin factor.

Numerical values of X_{NR} have been taken from Rosasco and Hurst [31].

The factor b is the Placzek-Teller coefficient [1] and is given by

$$b_J^{J+2} = \frac{3(J+1)(J+2)}{2(2J+1)(2J+3)}$$, for the O-branch (CSRS) and

$$b_J^{J-2} = \frac{3J(J-1)}{2(2J+1)(2J-1)}$$, for the S-branch (CARS).

γ^2_{00} is the anisotropy of the polarizability matrix elements and will be discussed in section iii:3.

V iii:2) Raman line widths

Raman line widths have been the subject of extensive experimental investigations. However few investigations have been performed for pure rotational Raman line widths [32-35]. The linewidths of the Raman Q-branch have thus been employed in the developed program package. The error thereby introduced is presumed to be small [5,22].

For N_2 and CO the Q-branch line widths (FWHM in cm^{-1}) have been found in a publication by Luthe [36] and are given there expressed in a convenient analytical expression (introduced by R.J. Hall [37]).

$$\Gamma(J,T,p) = (AT^a + BJT^b)p$$

The fitted constants for N_2 and CO are summarized in the following table.

Table 1. Q-branch Raman linewidth coefficients.

	A	a	B	b
N_2	5.97	-0.705	-3.95	-1.27
CO	13.78	-0.77	-4.052	-1.31

It is more common to use the rotational Raman line widths given by Jammu [32] for rotational CARS and extrapolate them assuming a $T^{-1/2}$ temperature dependence, to the appropriate temperature, J-number and pressure.

Q-branch line widths for O_2 will soon be published by Oazzany et al. [38] but in the present work the linewidths of O_2 have been assumed to be approximately identical to those of N_2 (see VI v:2).

V iii:3) Polarizability matrix elements

In the expression for the resonant non-linear susceptibility given in section V iii:1, the anisotropy of the polarizability matrix element, γ, was introduced. In this section the procedure of calculating the appropriate values of γ will be explained and some references given. The path followed is the one proposed by Drake [39]. In Ref. [39] γ is denoted β_v and an extra correction factor f(J) is introduced.

The f(J) term arises because as the molecule rotates rapidly in high rotational levels, its internuclear distance increases due to centrifugal effects. The effect on the rotational Raman cross-section can be determined, provided that the change in polarizability anisotropy with internuclear distance $(\delta\beta/\delta r)$ at the equilibrium position is known. (In the developed program this has not been considered and thus from here on $f(J)\equiv 1$. This is presumed to be a good assumption. See Ref. [40].)

In the same manner, molecular internuclear distances increase in higher vibrational levels because of vibrational anharmonicity resulting in

$$\beta_v = \beta_e + \beta'_e \langle r-r_e \rangle_v + 0.5\, \beta''_e \langle r-r_e \rangle_v^2 + \ldots$$

where

$$\langle r-r_e \rangle = r_e [(3B_e/\omega_e) + (\alpha_e/2B_e)](v+1/2).$$

A table of the constants above can be found in Ref. [39] for H_2, O_2, N_2 and CO.

V iii:4) CARS intensity convolutions

The quadruple integral to be calculated in the computer programs in the dual-broad-band case considered here is the following

$$I_{aS}(\omega_{aS}) = \int f^{slit}(\omega-\omega_{aS}) \iiint |X(\omega_{d1},\omega_{d2})|^2 I_d(\omega_{d1}) \; x$$
$$x \; I_d(\omega_{d2}) \; I_p(\omega_p) \; \delta(\omega_{d1}-\omega_{d2}+\omega_p-\omega_{aS}) \; d\omega_{d1} \, d\omega_{d2} \, d\omega_p$$

The non-linear susceptibility is given by

$$X = X^R(\omega_{d1}-\omega_{d2}) + X^{NR}$$

hence

$$|X|^2 = |X^R(\omega_{d1}-\omega_{d2})|^2 + (X^R)^2 + 2X^{NR} \, Re(X^R(\omega_{d1}-\omega_{d2}))$$

This means that

$$I_{aS}(\omega_{aS}) = (X^R)^2\langle 1\rangle + 2X^{NR}\langle ReX^R(\omega_{d1}-\omega_{d2})\rangle + \langle |X^R(\omega_{d1}-\omega_{d2})|^2\rangle$$

where

$$\langle F\rangle = \int f^{slit}(\omega-\omega_{aS}) \iiint F(\omega_{d1},\omega_{d2}) \; I_d(\omega_{d1}) \; x$$
$$x \; I_d(\omega_{d2}) \; I_p(\omega_p) \; \delta(\omega_{d1}-\omega_{d2}+\omega_p-\omega_{aS}) \; d\omega_{d1} \, d\omega_{d2} \, d\omega_p$$

If we, for a moment, disregard the slit-function convolution we still have a time-consuming numerical double integral. In order to reach reasonable execution times we need some closed-form solution. This can be achieved by assuming analytical spectral laser profiles (see V.iv.). By following the procedure introduced by Greenhalgh and Hall [41] using Gaussian laser profiles and the complex error function w, the integral above may be written

$$I_{aS}(\omega_{aS}) = \frac{I_d^{o\,2}\, I_d^{o}}{\sqrt{2\pi}.\Delta\omega_d} \cdot \exp\left[-\frac{(\omega_{aS}-\omega_p^{o})^2}{2\Delta\omega_d^2}\right].\{X_{NR}^2 - \frac{2\sqrt{\pi}}{\Delta\omega_p} X_{NR} \Sigma_i \mathrm{Im}(a_i w_i) +$$

$$+ \left[\frac{i\sqrt{\pi}}{\Delta\omega_p} \Sigma_j U_j a_j w_j + \text{c.c.}\right]\}$$

where

$$I_x(\omega) = \frac{I_x^{o}}{\sqrt{\pi}.\Delta\omega_x} \exp\left[-\frac{(\omega-\omega_x)^2}{\Delta\omega_x^2}\right] \quad , \; x=d,p \; ,$$

$$\Delta\omega_d >> \Delta\omega_p \quad , \quad \lambda''_j = -\Gamma_j \; , \; \lambda'_j = \omega_j \; ,$$

$$X(\Delta) = \Sigma_j \frac{a_j}{\lambda'_j - \Delta + i\lambda''_j} \quad , \qquad U_j = \Sigma_k \frac{a_k^{*}}{(\lambda'_k - \lambda'_j - i(\lambda''_k + \lambda''_j))} \quad ,$$

$$w(Z) = \frac{i}{\pi} \int_{-\infty}^{\infty} \frac{\exp(-t^2)}{Z - t}\, dt, \quad (\mathrm{Im}\, Z > 0) \quad ,$$

$$a_j = \frac{N}{\hbar} \Delta\rho_j^{(0)} \alpha_j^2$$

and $\Delta\rho_j^{(0)}$ = the normalized population difference,

ω_j = the Raman frequency for transition j,

$\hbar$ = Planck's const / 2π, Γ_j = the Raman line width for transition j,

α_j = polarizability matrix element for trans. j, N = the molecular number density.

Other articles treating intensity convolutions are [42-44] where [42] also gives expressions for non-Gaussian laser profiles.

V iv) Programs and data files

V iv:1) Generating theoretical spectra for plotting

Both CARS and CSRS spectra can be generated with the developed program package for any mixture of the gases N_2 ,O_2 and CO. When the experimental spectra are divided by a non-resonant CARS spectrum before the evaluation to compensate for the effects of the dye laser, the appropriate theoretical CARS spectrum should be generated with a sufficiently large input value of the dye laser width ($\Delta\omega > \omega$).

The input parameters are described in the computer code. The input file IN-POLYROT-CARS:SYMB (see Appendix III) is also in some sense self-instructing. After entering the input data into IN-POLYROT-CARS the generation of a spectrum file is performed by POLYROT-CARS. Plotting is thereafter controlled by the plotting program DNPLOT, utilizing the IGL graphic routines. (Examples of spectra generated by POLYROT-CARS and plotted by DNPLOT are given in figs 5.2-5.) (Both programs and the input file are stored under user ATOM-APPLICATION.)

V iv:2) Theoretical spectra for library generation

Before executing the temperature evaluation program ROTCARS-FIT, a theoretical rotational CARS spectrum library should be generated in a sufficiently large temperature and spectral interval. The generation is performed by ROTCARS-LIB after preparing the input file IN-ROTCARS-LIB:SYMB. The program can generate both CARS and CSRS spectra. The input parameters are described in the computer code. An inspection of the generated library files can be made by the plotting program DNPLOT. (The program is self-instructing and the files are stored under user ATOM-APPLICATION.)

V iv:3) The temperature evaluation program

The temperature evaluation program, ROTCARS-FIT, fits theoretical spectra calculated by ROTCARS-LIB to experimental, unformatted spectral files transferred from a PARC OMA-III multi-channel analyser, utilizing a fitting algorithm by Marquardt [45]. (The procedure used to transfer files from an OMA-III is described in Appendix II.) The input parameters are stored in an input file, e.g. IND-ROTCARS-FIT:N2, and the fitting program itself is stored in the file ROTCARS-FIT:SYMB. All files are available from user ATOM-APPLICATION and a complete description of the input parameters is provided in the computer code.

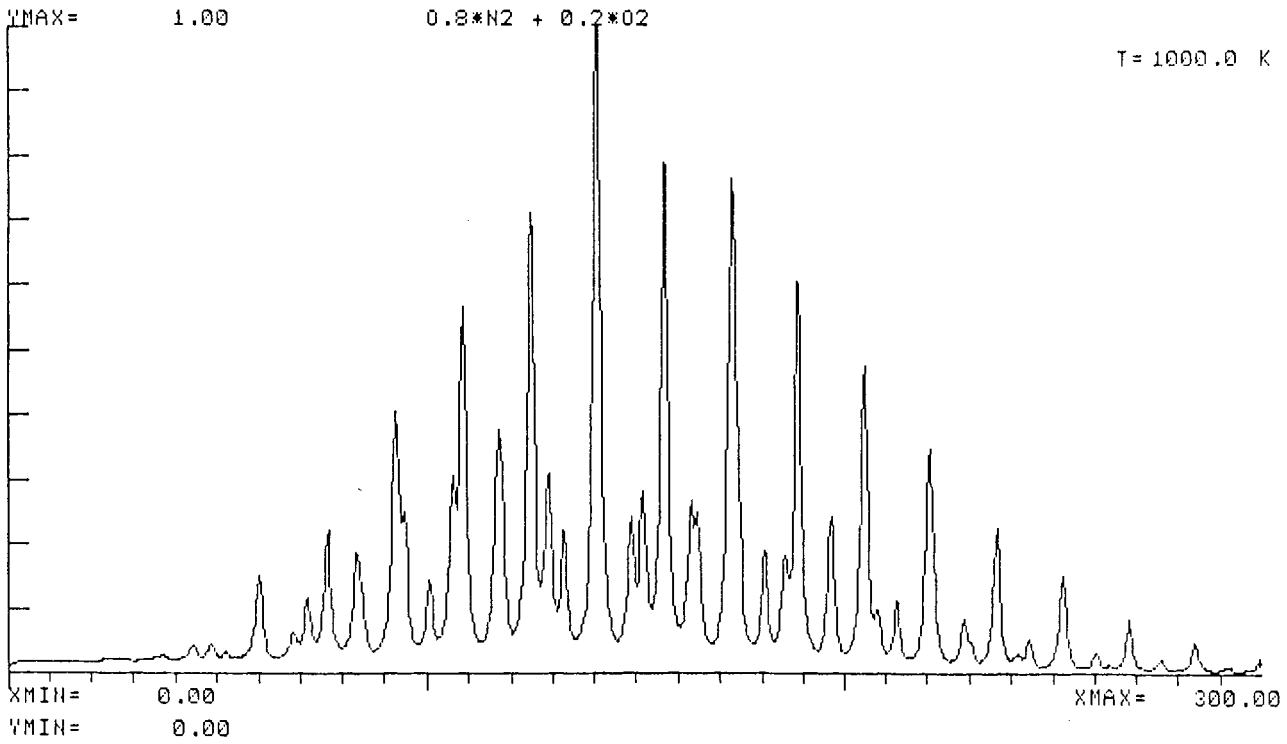

Fig. 5.2. Theoretically generated rotational CARS spectrum for air.

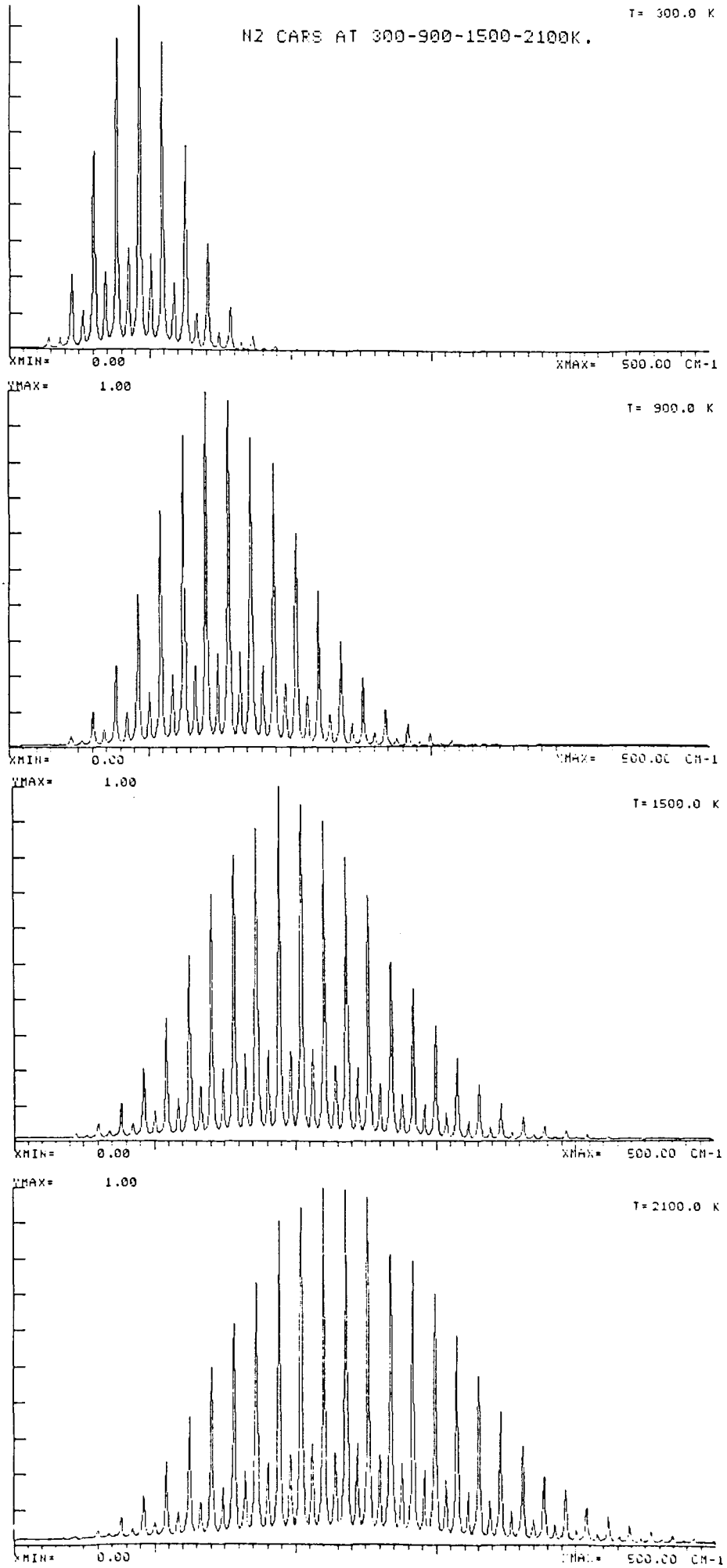

Fig. 5.3. Theoretical rotational CARS spectra of nitrogen at different temperatures.

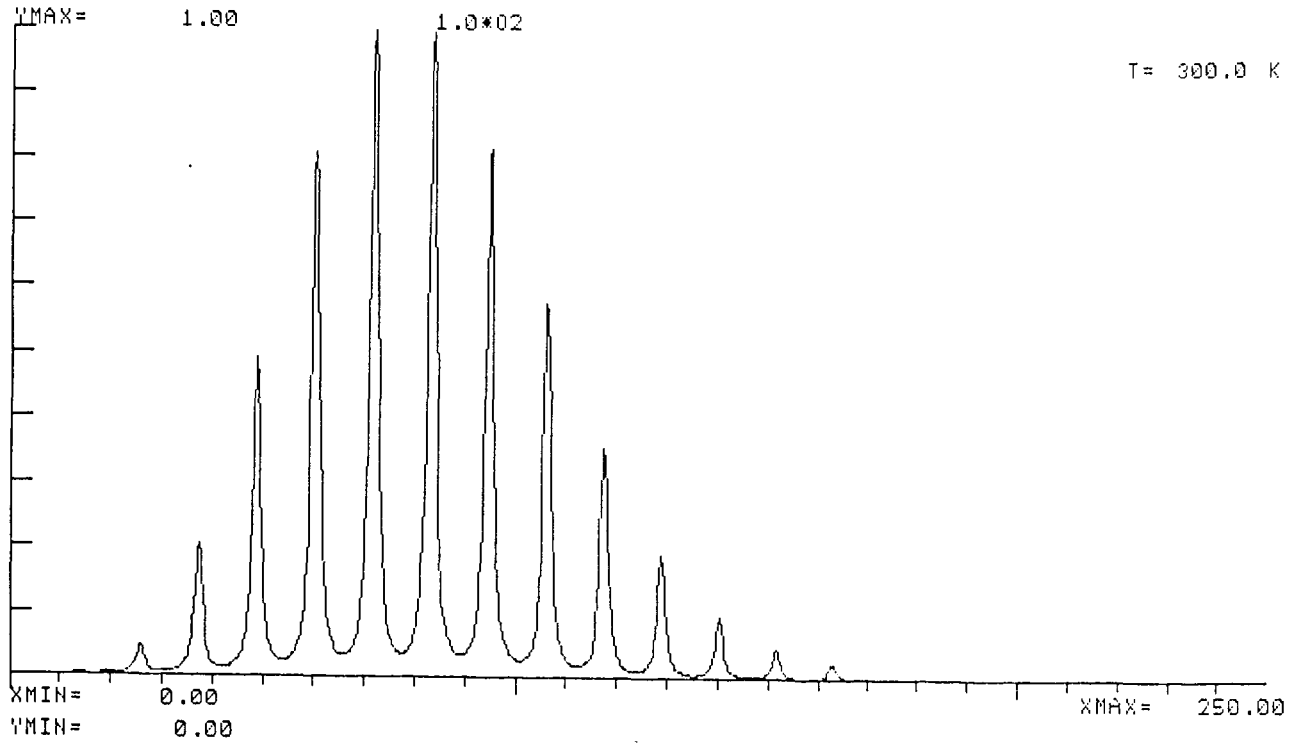

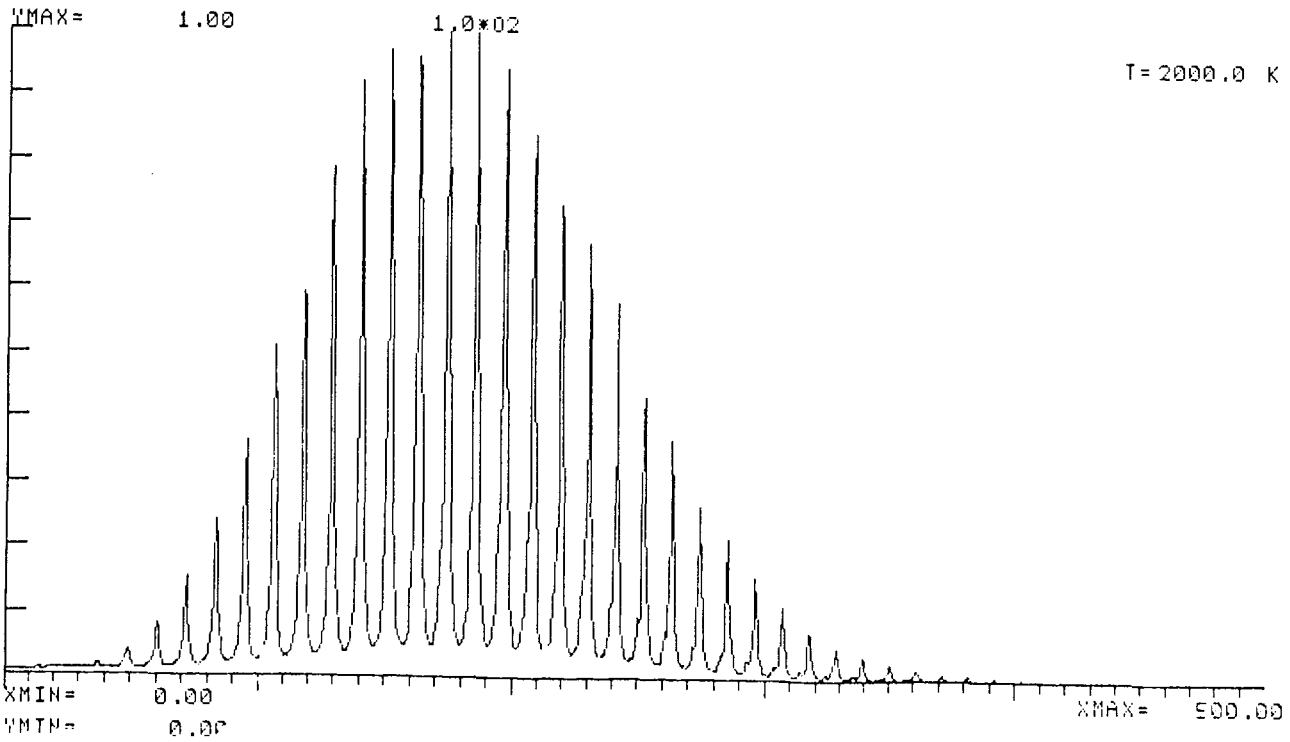

Fig. 5.4. Theoretical rotational CARS spectra of oxygen at different temperatures.

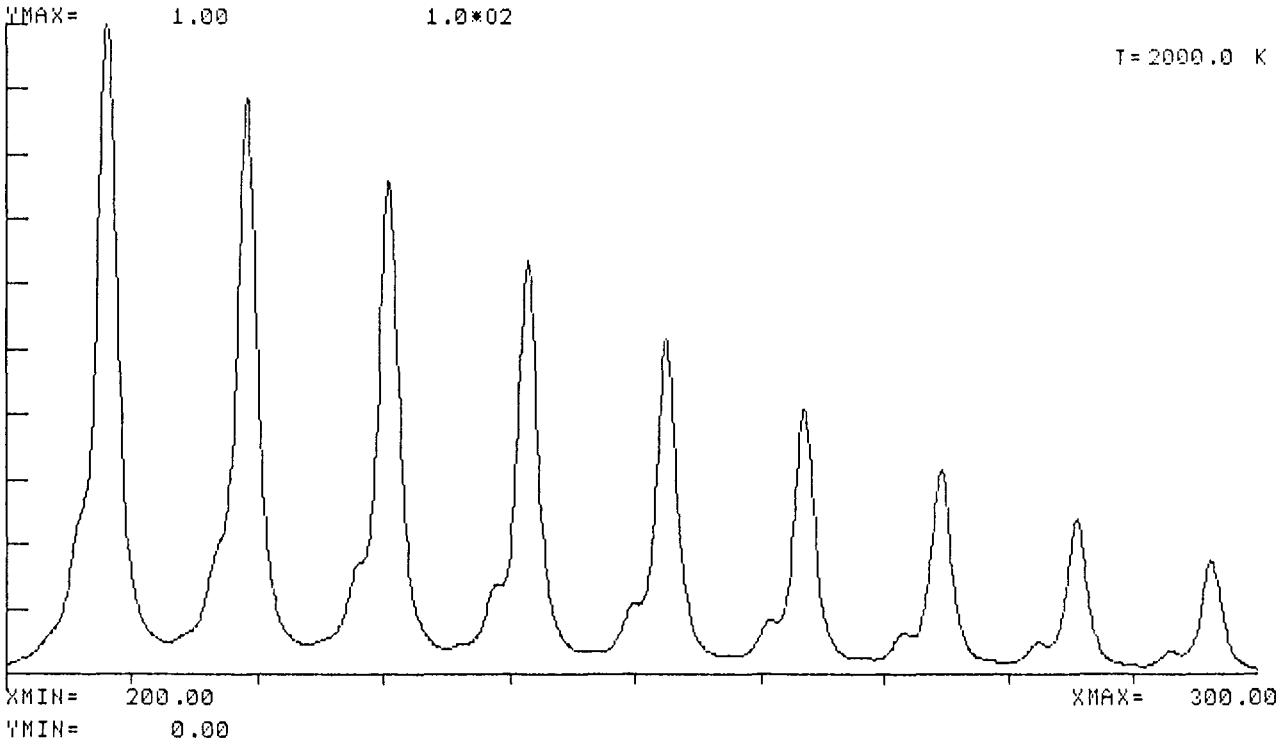

Fig. 5.5. Theoretical rotational CARS spectra of oxygen illustrating the presence of hot bands. (See chapter II.)

V v) Experimental results

V v:1) Introduction

The developed computer program package for generating theoretical rotational CARS spectra and for evaluating temperatures from experimental spectra has been tested and applied to some fields of interest. Firstly, as a result of earlier experiments performed at the department, some rotational CARS N_2 and O_2 spectra were available on floppy disc. These spectra were recorded with specified temperatures and have served as a test of the accuracy of the evaluation. Secondly, a short study of dye noise effects on the deduced temperature has been performed.

In order to run the fitting (evaluation) program the following input parameters are required. First, approximate values of the dispersion and the spectral position of a reference point are needed, but more important are the data describing the background susceptibility and the width and form of the instrumental slit function because these parameters are not fitted in the program. A finite background susceptibility, X_{NR}, results in a spectrum with a background and asymmetrical resonance peaks (see Ref. [22], p.226). The slit function is more crucial for the evaluation (at least at low temperatures). The existing program can perform a convolution with Gaussian, Lorentzian or triangular functions. An experimental function would probably be superior but unfortunately no experimental slit function was available and the second best alternative, a Lorentzian, was employed. (This was considered superior to the Gaussian function since it resulted in a better spectral fit.) As an alternative, a Voigt slit function, using the complex error function could be implemented and is assumed to give somewhat improved results.

V v:2) Evaluation of experimental spectra

The experimental spectra (CSRS, see chapter III) had been collected under the following conditions

(1) Oxygen, room temperature, 1 spectrum (10 shots),
(2) Oxygen, room temperature, 10 spectra (single shots),
(3) Nitrogen, room temperature, 1 spectrum (100 shots),
(4) Oxygen, different temperatures, 100 shots each.

Spectrum (1) was used to deduce an average oxygen temperature and spectra of type (2) were then used to deduce the single-shot standard deviations in temperature. The results showed a surprisingly low mean fitted temperature of 285K. The reason for this has not yet been fully understood. One source of error is the Raman linewidths of O_2 which have been assumed to be identical to those of N_2 (see section V iii:2), due to lack of experimental data. The consequences of this rather unmotivated assumption have not been studied. It has also been assumed that the dye laser profiles were Gaussian which might not have been correct (see section VI iv). In spite of this malfunction of the fitting program the noise measurements were continued and considered to give reliable results. The standard deviation in temperature was determined to be 14 K, corresponding to 4.8% noise in a single-shot, room-temperature measurement (see fig. 5.6).

Spectrum (3) was used to test the temperature evaluation in nitrogen. The fitted temperature was found to be 307 K, which is almost as far from the correct temperature as the O_2 deduction, but in the opposite direction (see fig. 5.7).

The oxygen spectra from higher temperatures were also examined but were found to be difficult to evaluate because of the high background resulting from the effects of the simultaneous rotational and vibrational CARS experiment (see Ref. [5] and fig. 5.8).

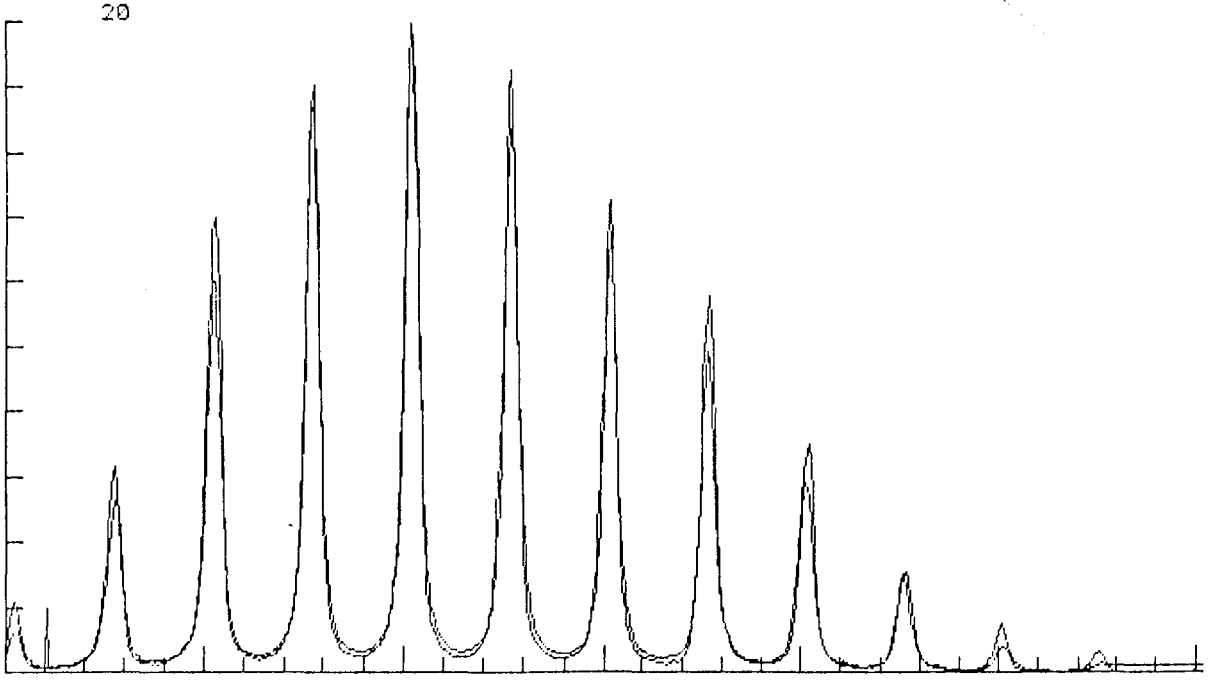

Fig. 5.6. Fitted and experimental oxygen spectra.

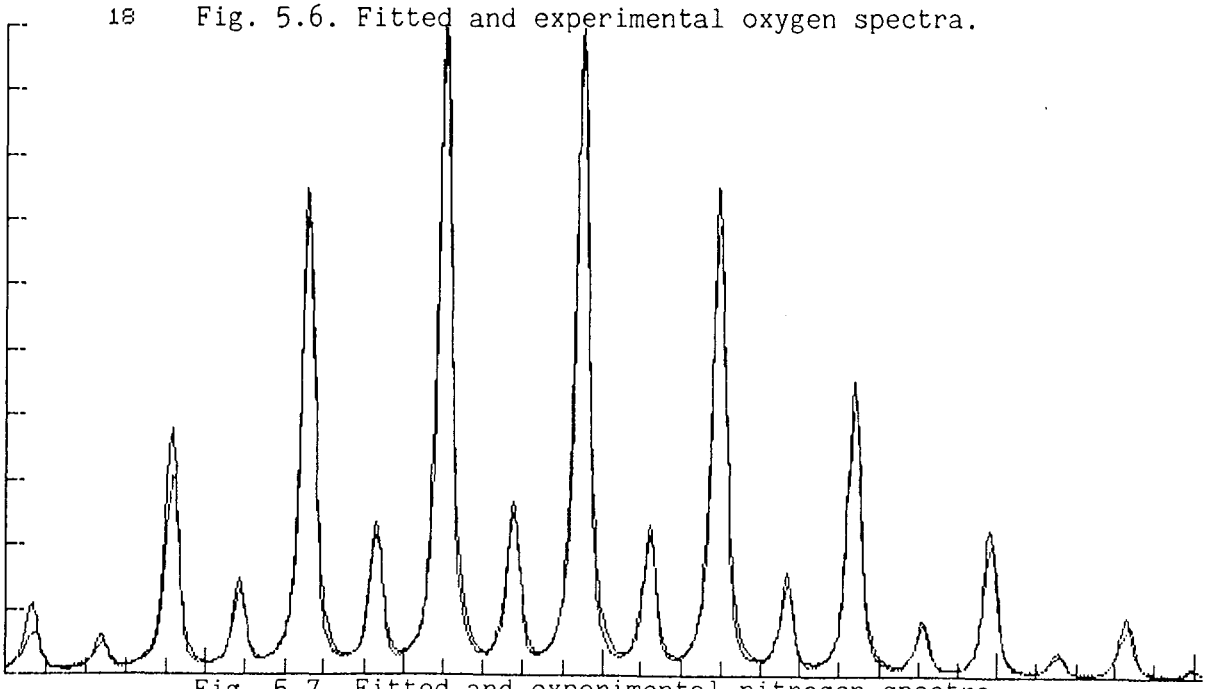

Fig. 5.7. Fitted and experimental nitrogen spectra.

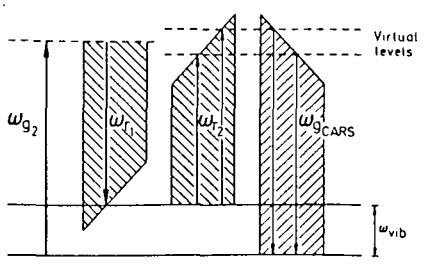

Fig. 5.8. Energy-level diagram for generation of a broadband background CARS signal.

V v:3) Effects of width fluctuations on temperature evaluation

The effects of a non-constant dye-laser spectral width have been briefly investigated by fitting theoretical spectra, generated for different dye-laser widths, to the experimental nitrogen spectra used before.

The nitrogen spectrum was recorded using a DCM dye with a broad-band width of 318 cm^{-1}. The results are summarized in the table below.

Table 2. Effects of width fluctuation of the DCM dye on the deduced temperature.

Width (cm^{-1})	250	290	310	314	318	325	340	370
Wid.dev. (%)	21.4	8.8	2.5	1.3	0	2.2	6.9	16.4
Fit.temp. (K)	317.0	310.1	307.6	307.2	306.8	306.1	304.8	302.7
Temp.dev. (%)	3.3	1.1	0.3	0.1	0	0.2	0.6	1.3

From the results above, a reasonable assumption is that the deduced temperature is relatively insensitive to width fluctuations. We are planning a more thorough examination of the effects of width fluctuations by fitting theoretical spectra with deviating widths to other theoretical spectra in the library.

V v:4) Effects of spectral dye noise on temperature evaluation

The effects of spectral dye noise have not been examined in this work but theoretical predictions have recently been made by S. Kröll et al. [46,47]. There it can be noted that the noise effects are reduced in the dual-broad-band approach compared with the conventional approach. Other publications treating CARS noise are [48,49].

VI. Effects of dyes in temperature evaluation

VI i) Dye properties of interest for CARS

When applying rotational CARS for single-shot flame temperature measurements either two different dyes can be employed, or one extremely broad and sufficiently efficient dye has to be provided. (Spectral width $\Delta\sigma$=400 cm^{-1}.)

The broadest dye now available seems to be DCM which, dissolved in the unpleasent solvent DMSO, reaches a width of 350 cm^{-1} [4]. One possible improvement would be if a mixture of two dyes resulted in a spectral profile consisting of one broad profile or two separated peaks. This will be further discussed in section VI ii).

Another important property of a dye suitable for the generation of single-shot rotational CARS spectra is the shape of the profile and the stochastic variations in the width. In the program for generating theoretical spectra a Gaussian shape with a fixed width is assumed. The error induced by the fluctuations in width is important for judging the accuracy in the temperature determination. The spectral shapes will be analysed in section VI iv) and the width fluctuations in section VI iii). The final property to be observed is the noise in the dye profile. This will be dealt with in section VI iii).

VI ii) Effects of dye mixing

One of the ways of expanding the temperature range suitable for rotational CARS temperature measurements would be by making dyes with broader spectral profiles available. The dye used today for higher temperatures, DCM, usually has a width (FWHM) of approximately 300 cm^{-1}. In order to measure, e.g., flame temperatures a "wider" dye would significantly improve the signal for large Raman shifts. In this diploma project I have, instead, studied the effects of dye mixing. The hope was that a binary mixture of dyes would result in a broader spectral profile.

The experimental set-up consisted of a Quanta-Ray PDL-1 dye laser pumped by a Quanta-Ray DCR-1 Nd:YAG laser, a spectrometer built at the institution and a PARC OMA-III detection system. In these experiments the dissolved dyes used in the noise measurements (see section VI iii).) were again used. This time, one of the solutions was poured into the dye pump system, the peak position and the half-widths (FWHM) were measured and the procedure was then repeated with portions of a different dye solution added. The number of experiments was limited by the quantity of premixed solutions available to 5 binary mixtures mixed in 2-7 different proportions each.

It should be mentioned that no effort was made to optimize the mixtures with respect to solvent, except for the previous optimization of the individual solutions. For the mixtures I have studied, some broadening was observed but when one of the components of the mixture was the broad dye DCM, unfortunately only reductions of the width were observed. One of the effects of the mixing was that a nearly linear interpolation in the spectral peak position was observed for the mixture relative to the unmixed components. This suggests dye mixing as a possibility when no single dye is available in a certain spectral region. The diagrams based on the rather limited experimental material can be seen in figure 6.1.

The noise properties of one of the dye mixtures was also examined. It was difficult to determine whether the mixing resulted in reduced or increased noise. (See section VI iii).)

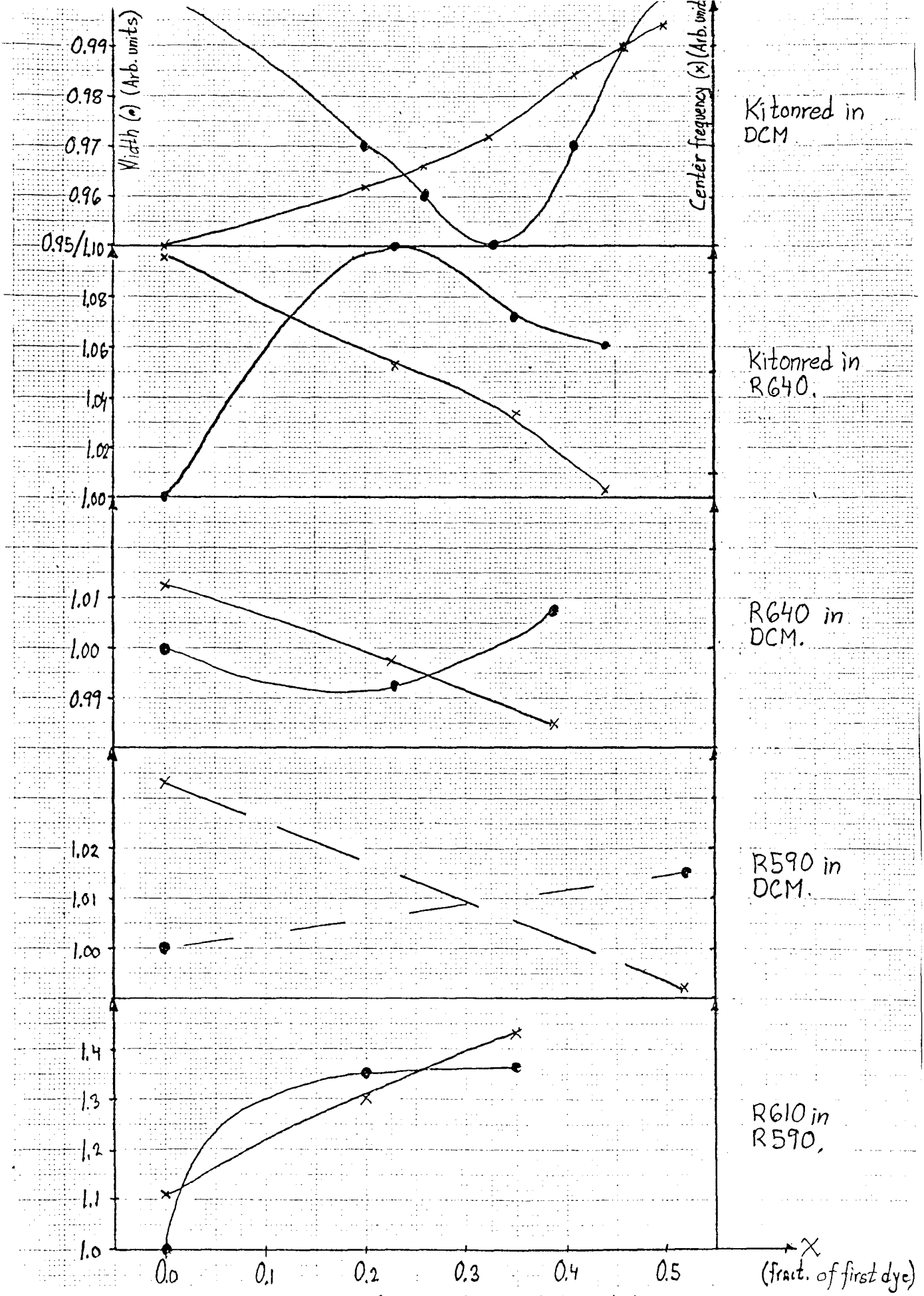

Fig. 6.1. Effects of dye mixing on width and peak position.

VI iii) Measurements of dye noise and width fluctuations

The noise properties of six different dyes and one of the dye mixtures have been studied. The noise was separated into two supposingly independent parts; one describing the stochastic width fluctuation observed at low dispersion, and the other describing the finer pixel-to-pixel noise, hereafter called "noise", studied at large dispersion (high resolution). The experimental set-up was the same as described in page 29.

The width fluctuation was studied by collecting 25 single-shot spectra at low dispersion. (Some of the collected single-shot spectra can be seen in fig. 6.2.) A program was then run on an OMA-III measuring the FWHM (full width at half maximum) and calculating the standard deviations. The dispersion of the spectrometer had been determined in an earlier experiment.

The results can be seen in the table below. The examined dyes are Rhodamine 590 (R590), R610, R640, DCM, Fluorescein, Kitonred and a mixture of R610 and R590.

Table 3. The width and width fluctuations in several dyes.

Dye	R590	R610	R640	DCM	Fluore	Kitonr	Mixt.
Width (cm^{-1})	141	130	131	279	144	117	168
Wid.noise(%)	2.8	3.8	7.6	4.3	1.8	5.3	9.5

It should be noted that the experimental material is small and that the short lifetime of the dye Fluorescein resulted in a rapid decrease in power during the experiment.

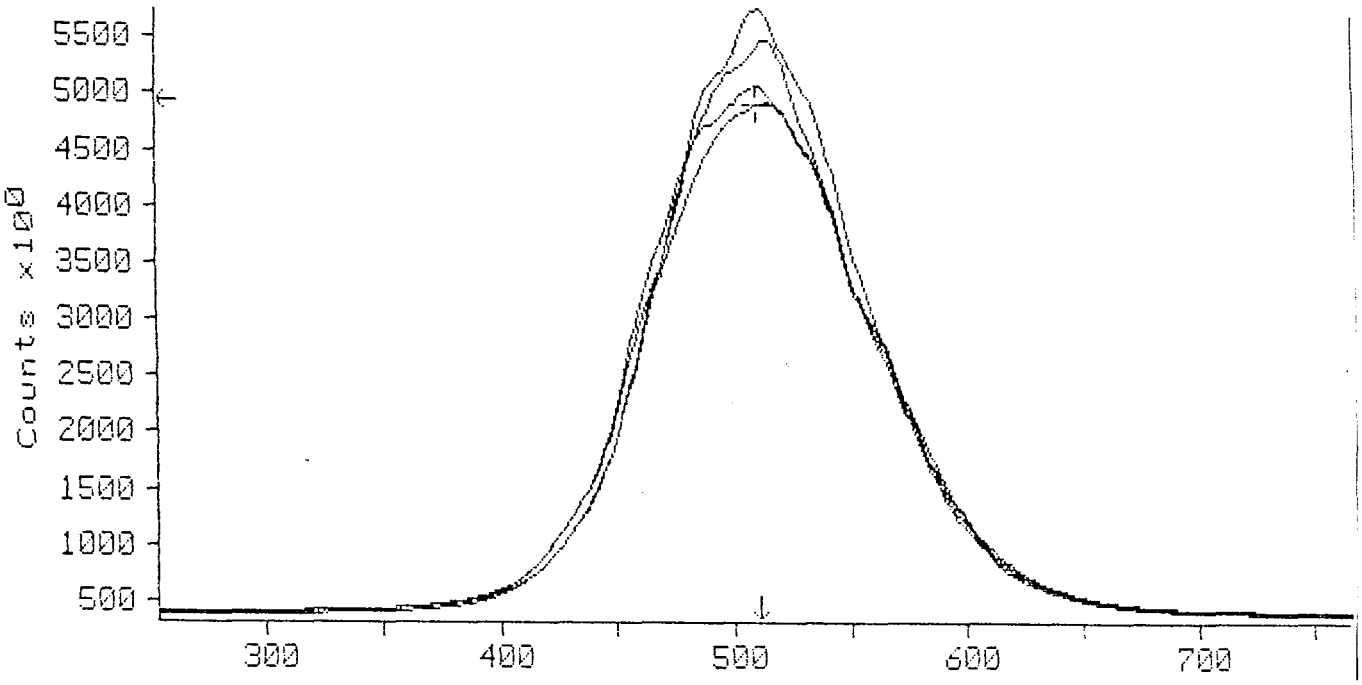

Fig. 6.2. Single-shot spectra showing width fluctuations.

The measurements were complicated by some regular variations in the spectra. During the measurements on one dye, every third spectrum showed a significantly larger width. In another dye, three wider spectra followed three narrower ones. These effects are assumed to be caused by regular variations in the old pump laser (Nd:YAG) and were not included in the noise.

The noise was studied in a high dispersion order of the spectrometer grating. One accumulated 100-shot spectrum and 25 single-shot spectra were recorded. (Some single-shot spectra are shown in fig. 6.3.) By dividing the single-shot spectra by the accumulated spectrum a curve, as in fig. 6.4 is obtained.

The standard deviation of the normalized, divided curve was calculated over 400, 100 and 50 pixels for all dyes and the results are given in table 4. The idea of performing the calculations over different numbers of pixels is to consider both the contribution of multi-pixel fluctuations (of importance over a larger region e.g. 400 pixels), and the disadvantages of a small statistical material. This procedure was followed for all dyes and the results can be seen in the table below.

Table 4. Pixel-to-pixel noise (%) and SD (%) for some dyes.

Pixels/Dye	R590	R610	R640	DCM	Fluore	Kitonr	Mixt.
50 pixels	4.6:1.2	4.3:1.0	4.4:1.1	6.4:2.0	4.2:1.1	3.6:1.0	4.3:1.1
100 pixels	4.8:0.7	4.8:0.8	5.3:1.3	7.6:2.1	4.6:1.1	4.0:1.1	4.9:0.9
400 pixels	4.9:0.5	6.7:1.4	7.6:1.9	9.8:2.3	4.9:0.6	5.4:1.3	6.5:0.8

(Fluore=Fluorescein, Kitonr=Kitonred, Mixt=Mixture of R610 and R590)

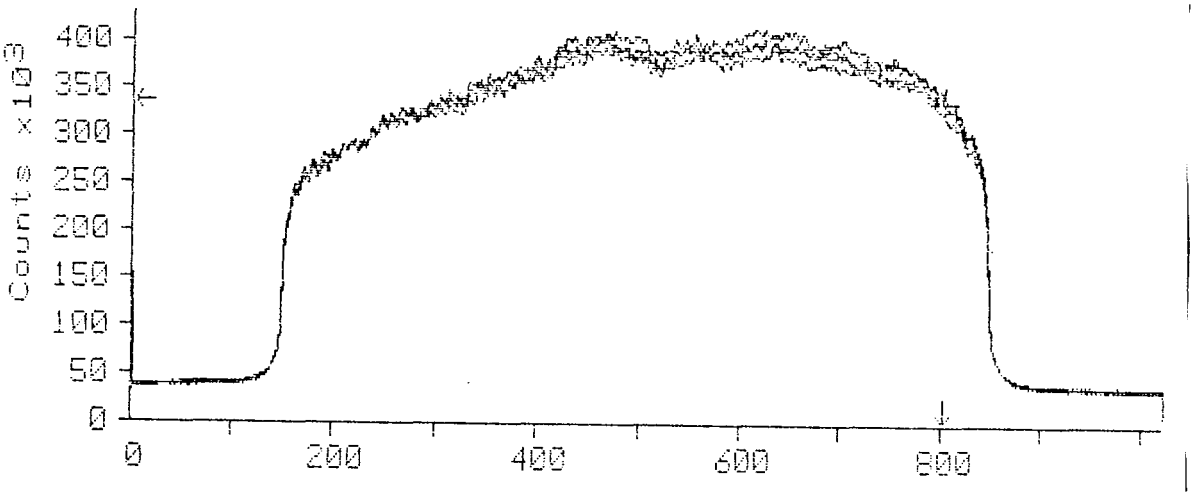

Fig. 6.3. Single-shot spectra showing the dye noise.

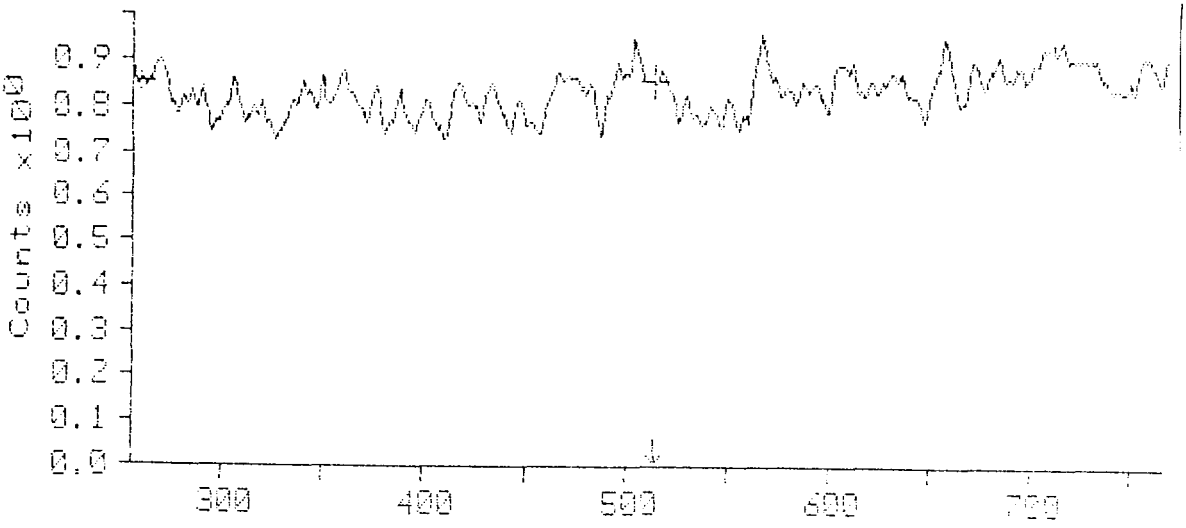

Fig. 6.4. Divided spectra for noise determination.

VI iv) Spectral profiles of dyes

The shapes assumed for the spectral dye profiles have a significant influence on the shapes of the theoretical spectra generated by the computer programs. Considerable simplifications are achieved if either Gaussian or Lorentzian dye profiles can be assumed.

Since the spectral shapes of some common dyes were already available from the study of width fluctuations a quick study of the profiles was possible. This was done by comparing the averaged spectra collected earlier with Gaussian curves with identical amplitudes and widths. The results are shown in fig. 6.5. (The crosses represent the Gaussian values.) As can be seen, most curves show satisfactory agreement. A complication that occasionally occurred in some spectra was a periodical structure in the curve, probably due to some Fabry-Perot interference phenomenon. This is probably the majorcause of the deviation from Gaussian shapes. An estimation of the thickness of the layer responsible was made by applying the Fabry-Perot formula

$$\Delta\lambda = \lambda^2 / 2nd.$$

This resulted in an estimated thickness of the interfering layer of d=0.2 mm. For the single-shot profiles the situation is different, with much larger deviations from ideal Gaussian shapes.

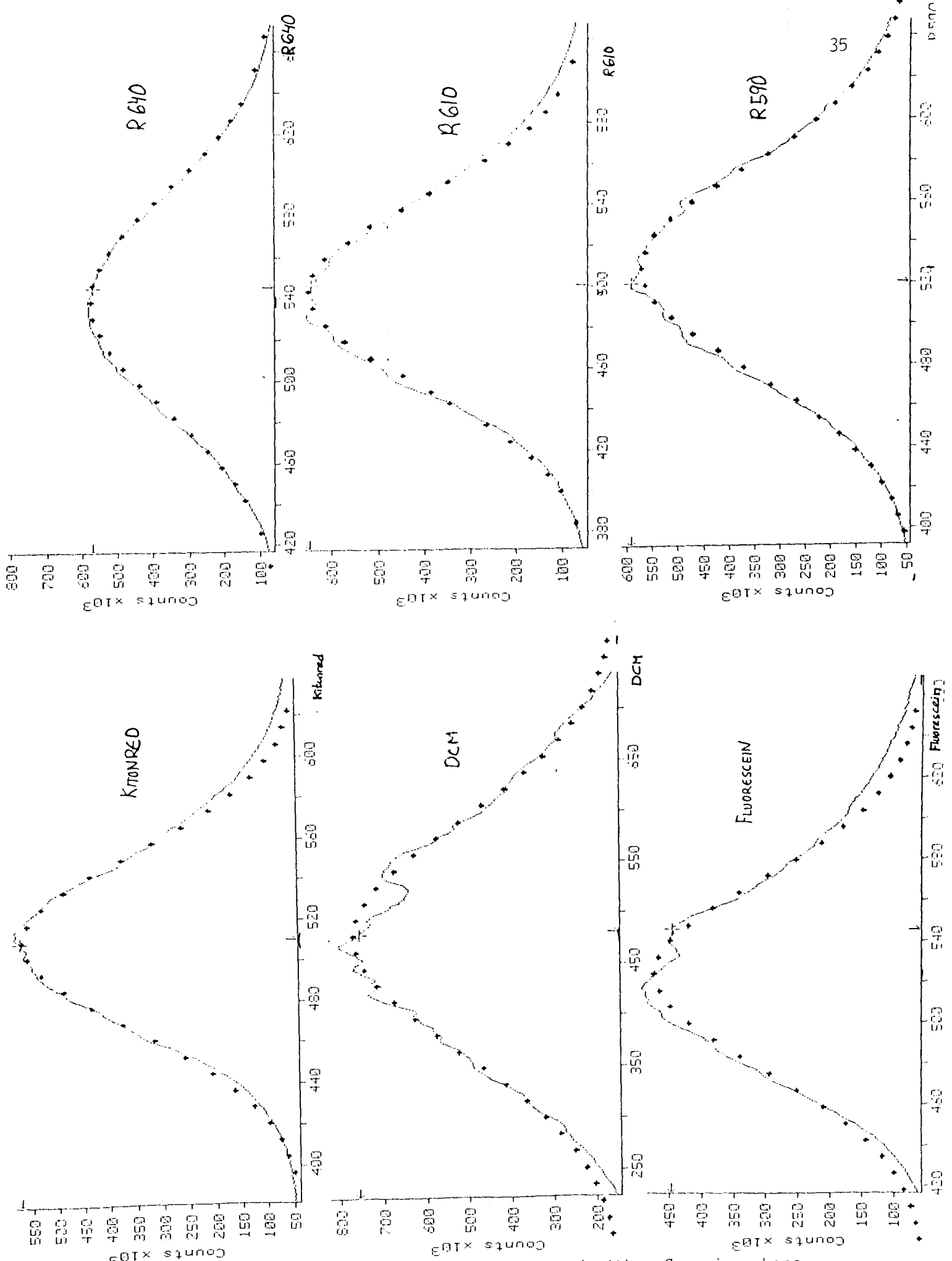

Fig. 6.5. Some dye profiles compared with a Gaussian shape.

VII. Acknowledgements

I wish to acknowledge those who in different ways have contributed to this diploma project; Hans Hertz for his advise when selecting an interesting project, Dr Marcus Aldén and Dr Stefan Kröll as encouraging supervisors and Lars Gramstad for his help when gold coating the laser flash-lamp mirrors (see Appendix I).

VIII. References

1. G.Herzberg, Molecular Spectra and Molecular Structure, I, Spectra of Diatomic Molecules (Van Norstrand,New York, 1950),
2. T.Parameswaran, D.R.Snelling, DREO technical note 81-18 (1982),
3. P.D.Maker and R.W.Terhune, Phys.Rev., 137,A801 (1965),
4. A.C.Eckbreth, T.J.Andersson, Opt.Lett., 11,496 (1986),
5. M.Aldén, P.E.Bengtsson and H.Edner, Appl.Opt., 25,4483 (1986),
6. J.J.Barrett, Appl.Phys.Lett., 29,722 (1976),
7. J.B.Zheng, J.B.Snow, D.V.Murphy, A.Leipertz and R.K.Chang, Opt.Lett., 9,341 (1984),
8. D.V.Murphy, R.K.Chang, Opt.Lett., 6,233 (1981),
9. L.P.Goss, J.W.Fleming and A.B.Harvey, Opt.lett., 5,345 (1980),
10. M.Aldén, L.R.A.P.-16, (Lund Reports on Atomic Physics), (1982),
11. J.B.Zheng, A.Leipertz, J.B.Snow and R.K.Chang, Opt.Lett., 8,350 (1983),
12. I.R.Beattie, T.R.Gilson and D.A.Greenhalgh, Nature 276,378 (1978),
13. C.M.Roland and W.A.Steele J.Chem.Phys., 73,5919 (1980),
14. J.A.Shirley, R.C.Hall and A.C.Eckbreth, Opt.Lett., 5,380 (1980),
15. Y.Prior, Appl.Opt., 19,1741 (1980),
16. Y.R.Shen, The Princ. of Nonlinear Optics, John Wiley & Sons, Inc., (1984),
17. R.J.Hall, L.R.Boedecker, Appl.Opt., 23,1340 (1984),
18. P.R.Regnier and J.P.E.Taran, Appl.Phys.Lett, 23, 240 (1973),
19. P.R.Regnier, F.Moya and J.P.E.Taran, AIAA J. 12,826 (1974),

20. M.Aldén, H.Edner and S.Svanberg, Phys.Scripta, 27,29 (1983),
21. R.E.Teets and J.H.Bechtel, Opt.Lett., 6,458 (1981),
22. R.J.Hall and A.C.Eckbreth, Laser Applications vol 5, Edited by J.F.Ready and R.K.Erf, Academic Press, New York, (1984),
23. L.P.Goss, J.W.Fleming and A.B.Harvey, Opt.Lett., 5,345 (1980),
24. M.Aldén, private comm.,
25. A.Leipertz and E.Magens, AIAA-85-1569,
26. D.V.Murphy and R.K.Chang, Opt.Lett., 6,233 (1981),
27. J.Doppelbauer and G.Leyendecker, Appl.Spectr. 40,881 (1986),
28. M.Pealat, P.Bouchardy, M.Lefebvre and J.-P.Taran, Appl.Opt., 24,1012 (1985),
29. B.Dick and A.Gierulski, Appl.Phys.B, 40,1 (1986),
30. T.R.Gilson, I.R.Beattie, J.D.Black, D.A.Greenhalgh and S.N.Jenny, J.of R.Spectr., 9,361 (1980),
31. G.J.Rosascu and W.S.Hurst, Phys.Rev., A32,281 (1985),
32. K.S.Jammu, G.E.St.John and H.L.Welsh, Can.J.of Phys, 44,797 (1966),
33. M.Bérard, J.P.Cèbe, M.Giraud and P.Lallemand, Proc. of the 8th ICORS - Bordeaux,France (1982),
34. H.G.M.Edwards, D.A.Long and S.W.Webb, Proc. of the 9th ICORS - Tokyo,Japan (1984),
35. H.G.M.Edwards, D.A.Long and G.Sherwood, Proc. of the 10th ICORS - Eugene,USA (1986),
36. J.C.Luthe, E.J.Beiting and F.Y.Yueh, Comp.Phys.Comm., 42,73 (1986),
37. R.J.Hall, Appl.Spectr., 34,700 (1980),
38. Y.Oazzany, J.P.Boquillon and B.Lavorel, Can.J.of Phys, to be published,
39. M.C.Drake, Opt.Lett., 7,440 (1982),
40. M.C.Drake, C.Asawaroengchai and G.M.Rosenblatt, Laser probes for comb. chem., Edited by D.R.Crosley, ACS Symp. Series 134,

41. D.A.Greenhalgh, R.J.Hall, Opt.Comm., 57,125 (1985),
42. F.Y.Yeuh and E.J.Beiting, Comp.Phys.Comm., 42,65 (1986),
43. R.J.Hall, Opt.Comm., 52,360 (1985),
44. R.E.Teets, Opt.Lett., 9,226 (1984),
45. Marquardt, J.Soc.Ind.Appl.Math., 11,431,
46. S.Kröll, M.Aldén, T.Berglind and R.J.Hall, Appl.Opt., 26,1068 (1987),
47. S.Kröll and D.Sandell, To be published,
48. D.R.Snelling, R.A.Sawchuk and R.E.Mueller, Appl.Opt., 24,2771 (1985),
49. D.A.Greenhalgh and S.T.Whittley, Appl.Opt., 24,907 (1985),
50. C.M.Penney, R.L.St.Peters and M.Lapp, J.Opt.Soc.Am., 64,712 (1973).

Appendix I. Gold coating of laser flash lamp mirrors

In one of the experiments using the Nd:YAG laser the power was surprisingly low and therefore the boxes surrounding the YAG rods and the flashlamps were removed. The mirrors, made of brass and covered by a thin gold coating, proved to be affected and were coated by a film, supposedly some oxide.

By evaporation of gold in a high-vacuum system, the coating was renewed and an increase in the laser power was realized.

Appendix II. Transferring files from an OMA-III to the ND computer

The transfer of data files from a PARC OMA-III multi-channel analyser to a ND computer is performed in four steps

1) The transferring programs cannot deal with OMA files divided into several memories. Before continuing each spectrum should be placed in a separate file on the floppy disc.
2) After connecting the OMA to a PC and placing the OMA in the "PRINTER" menu the transfer to the PC is handled by the program TRANSFER.
3) The transfer from the PC to the ND computer is handled by ND-link and PC-link.
4) The ASCII files are convered into unformatted real files by the program OMA-ASCII-REAL.

The transferring programs were provided by S. Kröll and the appropriate version of OMA-ASCII-REAL is stored under user ATOM-APPLICATION.

Appendix III. Input file for the program POLYROT-CARS

DATA					; EXPLANATION	; REF
*** GENERAL DATA FOR POLYROT-CARS ***					;	;
CARS					; CARS or CSRS	;
15625.	317.6	18797.	0.8		; dye/pump-fr/wid	;
18797.	19297.				; interval (cm-1)	;
1.00	0.00	0.00			; xmol:N2 O2 CO	;
2100.	1.0				; temp(K),press	;
0.94830+27					; susc.const	;
L	1				; slit:type,no,	;
1.4	2.	2.7			; widths	;
					;	;
*** N2 DATA ***					;	;
5.97	-.705	-3.95	-1.27		;Q Raman widths	;Lu
2358.5849	14.33245	-.002106	0.0002583		;we,xwe,ywe,zwe	;
2.02276	5.951-06	.0172978	-.0000415	8.32000-09	;Be,De,B1,B2,D1	:Gi
6.	3.				;Nucl weights;e,o;	
1.09768-08	6.91-25	1.4-16	0.		;re,bet,bet',bet"	;He,Dr
0.82-17					;NR susc	;
					;	;
*** O2 DATA ***					;	;
5.97	-.705	-3.95	-1.27		; same as N2	;
1580.19	11.98	0.	0.		;	;He
1.44563	4.839-06	0.0159	0.	0.	;	;He
0.	1.				;	;?
1.20752-08	10.80-25	3.89-16	0.		;	;He,Dr
0.78-17					;	;Ru
					;	;
*** CO DATA ***					;	;
13.78	-0.77	-4.052	-1.31		;	;Lu
2169.81358	13.28831	0.	0.		;	;He
1.93128087	6.21214-06	0.01750441	0.	0.	;	;He
1.	1.				;	;
1.12832-08	5.25-25	1.72-16	0.		;	;He,Dr
0.82-17					; same as N2	;
					;	;

REFERENCES :
He = Huber/Herzberg
Dr = Drake, Opt Lett,Vol 7,No 9,1982
Lu = Luthe et al,
Ru = Rus.&Hur.,Phys.Rev.,A32,281,(1985)
Gi = Gibson,J.of R.Spectr.,9,361,(1980)